Fully Tunable Hyperfine Interactions of Hole Spin Qubits in Si and Ge Quantum Dots

Stefano Bosco* and Daniel Loss
Department of Physics, University of Basel, Klingelbergstrasse 82, 4056 Basel, Switzerland

(Received 25 June 2021; accepted 13 October 2021; published 3 November 2021)

Hole spin qubits are frontrunner platforms for scalable quantum computers, but state-of-the-art devices suffer from noise originating from the hyperfine interactions with nuclear defects. We show that these interactions have a highly tunable anisotropy that is controlled by device design and external electric fields. This tunability enables sweet spots where the hyperfine noise is suppressed by an order of magnitude and is comparable to isotopically purified materials. We identify surprisingly simple designs where the qubits are highly coherent and are largely unaffected by both charge and hyperfine noise. We find that the large spin-orbit interaction typical of elongated quantum dots not only speeds up qubit operations, but also dramatically renormalizes the hyperfine noise, altering qualitatively the dynamics of driven qubits and enhancing the fidelity of qubit gates. Our findings serve as guidelines to design high performance qubits for scaling up quantum computers.

DOI: 10.1103/PhysRevLett.127.190501

Introduction.—Spin qubits in hole quantum dots are leading candidates to process quantum information [1–5]. Elongated hole quantum dots hold particular promise because of their large and tunable direct Rashba spin-orbit interaction (DRSOI) [6–9]. This property enables fast all-electric gates [10–15] via electric dipole spin resonance (EDSR) [16–19] and could pave the way towards scalable quantum computers. A major source of decoherence in these qubits comes from the hyperfine interaction between the confined hole and the nuclear spins. Isotopic purification could decrease the number of nuclear defects by 2 [20,21] to 3 [22] orders of magnitude, however, this procedure is expensive and not routine in state-of-the-art devices, where hyperfine noise still drastically limits the qubit performance [13].

The hyperfine interactions in hole nanostructures originate from dipolar coupling [23–29] and in Si and Ge their amplitude is predicted to be comparable to electrons [30,31]. In contrast to electrons [32–34], however, these interactions are strongly anisotropic, approaching the Ising limit in planar structures [29,35]. Ising coupling causes a slow power-law spin decay depending on the orientation of the field [36,37] and could result in an enhancement of the qubit lifetime when the nuclear spins are suitably prepared [38–42].

In this work, we show that in elongated hole quantum dots the amplitude of the hyperfine interactions as well as their anisotropy are fully tunable by external electric fields, resulting in devices with an order of magnitude smaller hyperfine noise. This decrease in noise can save 2 orders of magnitude of isotopic purification. Strikingly, by analyzing common designs, we find optimal working points in Si fin field effect transistors (FinFETs) [13,43,44] where both hyperfine and charge noise [45] are suppressed simultaneously, strongly boosting the qubit coherence. Also, we examine the interplay between DRSOI and hyperfine interactions [46]. The large DRSOI substantially renormalizes the hyperfine noise and qualitatively alters the spin dynamics in EDSR experiments, yielding more coherent qubit operations. We foresee that the tunability of the hyperfine interactions could be exploited also in hybrid systems [47] to engineer a coherent coupling between quantum dots and nuclear spin qubits [48–52].

Hyperfine interactions in elongated quantum dots.—Spin qubits confined in quantum dots are generally described by the effective Hamiltonian [26,27,29] $H_Q = (\boldsymbol{b}+\boldsymbol{h})\cdot\boldsymbol{\sigma}/2$, comprising a Zeeman field $\boldsymbol{b} = \mu_B \underline{g}\mathbf{B}$ and an Overhauser field $\boldsymbol{h} = \sum_k A_k \Gamma(\mathbf{r}_k)\mathbf{I}^k/n_0$. These fields model the magnetic interactions of the confined particle with an external magnetic field $\mathbf{B}$ and with an ensemble of nuclear spins $\mathbf{I}^k$ at position $\mathbf{r}_k$, respectively. Here, μ_B is the Bohr magneton, n_0 is the nuclear density, A_k is the hyperfine coupling strength, and we neglect small long-range corrections to the hyperfine interactions [29].

The microscopic properties of the system determine the values of the matrices $\underline{g}$ of g factors and $\Gamma(\mathbf{r}_k)$ of local spin susceptibilities. While in electron quantum dots these matrices are proportional to the identity matrix, resulting in isotropic interactions, in hole dots they have a richer structure and heavily depend on the mixing of heavy (HH) and light hole (LH) bands [53], that carry spin $3/2$ and $1/2$, respectively. In particular, HH dots have a strongly anisotropic g factor [54] and Ising hyperfine interactions $\propto \sigma_z h_z$ [26,27,29,55,56], while in LH dots the anisotropy is less pronounced and the transverse components $h_{x,y}$ of $\boldsymbol{h}$ are two times larger than h_z [30,57].

In this work, we analyze quantum dots that are tightly confined in the $\boldsymbol{\rho} = (x, y)$ plane and extend in the z

direction. In these systems, the HH-LH mixing can be engineered by designing the dot [8,45] and is highly tunable by external electric fields. It is accurately modeled by the Hamiltonian

$$H = H_{\rm LK} + V_C(\boldsymbol{\rho}) + \frac{\hbar\omega_z}{2l_z^2}z^2 - eE_y y, \tag{1}$$

which includes the Luttinger-Kohn Hamiltonian $H_{\rm LK}$ [53] and an electric field E_y perpendicular to the long direction. Here, the dot is defined by a harmonic potential with frequency ω_z and length l_z, and an abrupt potential $V_C(\boldsymbol{\rho})$. This potential models etched nanowires, but we emphasize that our theory also describes squeezed dots in planar heterostructures [9].

When the nanowires are grown along high symmetry axes, e.g., $z\|[001]$ or [110], the ground state Kramer partners $\Psi_{\uparrow\downarrow}$ of H are well approximated by $\Psi_{\uparrow\downarrow}\approx e^{-iz\sigma_x/l_{\rm SO}}\psi_{\uparrow\downarrow}(\mathbf{r})$, see Sec. I A of [58]. The spinors

$$\psi_\uparrow(\mathbf{r}) = \varphi(z)\left(\psi_H(\boldsymbol{\rho})\left|+\frac{3}{2}\right\rangle + \psi_L(\boldsymbol{\rho})\left|-\frac{1}{2}\right\rangle\right) = \mathcal{T}\psi_\downarrow(\mathbf{r}) \tag{2}$$

locally hybridize different eigenstates of the spin-3/2 matrix J_z by the spin-resolved and E_y-dependent wave functions $\psi_{H,L}(\boldsymbol{\rho})$. The time-reversal operator $\mathcal{T}$ flips the spin and complex conjugates the functions, and $\varphi(z)$ is the harmonic oscillator ground state. The spin-dependent local phase in $\Psi_{\uparrow\downarrow}$ accounts for the large DRSOI [6–9], which is parametrized by an E_y-dependent spin-orbit length $l_{\rm SO}$ typically of tens of nanometers [13,14]. Here, we compute $\psi_{H,L}$ and $l_{\rm SO}$ by numerically discretizing Eq. (1) in analogy to [45]. Because we only study dots where E_y is aligned to high symmetry axes, the DRSOI points in the x direction [6–8,45].

When $|\mathbf{B}| \lesssim 1$ T, the magnetic interactions are weaker than $\hbar\omega_z$ and by projecting the hyperfine $H_{\rm HF} = \sum_k \delta(\mathbf{r}-\mathbf{r}_k)A_k\mathbf{I}^k\cdot\mathbf{J}/2n_0$ [26,27,29,30,32] and Zeeman Hamiltonian $H_Z = 2\kappa\mu_B\mathbf{B}\cdot\mathbf{J}$ [53] onto $\Psi_{\uparrow\downarrow}$, we find [58]

$$\Gamma(\mathbf{r}) = |\varphi(z)|^2 R_x\left(\frac{2z}{l_{\rm SO}}\right)\begin{pmatrix} \mathrm{Re}[\gamma_+] & \mathrm{Im}[\gamma_-] & 0 \\ -\mathrm{Im}[\gamma_+] & \mathrm{Re}[\gamma_-] & 0 \\ 0 & 0 & \gamma_z \end{pmatrix}, \tag{3}$$

and $g_{ij} = 4\kappa\int d\mathbf{r}\Gamma_{ij}(\mathbf{r})$. Here, we neglect small corrections coming from terms $\propto J_i^3$ [30,53], $\propto 1/l_z^2$ [7,9,59], and from magnetic orbital effects [59,60]. We define $\gamma_\pm = \psi_L(\psi_L \pm \sqrt{3}\psi_H)$, $\gamma_z = (3|\psi_H|^2 - |\psi_L|^2)/2$, and $R_x(\theta)$ is an anticlockwise rotation matrix of an angle θ around x. This SOI-dependent rotation causes the well-known suppression $e^{-l_z^2/l_{\rm SO}^2}$ of the g factor [60,61], and also significantly alters the hyperfine interactions.

If no effort is put in preparing the state of the nuclear spins [38–41], the Overhauser field $\boldsymbol{h}$ is Gaussian distributed [32,33,37,62], and has zero mean and diagonal covariance matrix $\Sigma_{ij} = \hbar^2\sigma_i\delta_{ij}/\bar{\tau}^2$ [58]. The characteristic time of hyperfine-induced qubit decay is

$$\bar{\tau} = \frac{\hbar}{|A_k|}\sqrt{\frac{3N}{\nu I(I+1)}}, \tag{4}$$

where ν is the isotopic abundance of the nuclear defects, $N = \sqrt{2\pi}l_z\mathcal{A}_\rho n_0$ is the number of atoms in the dot, and $\mathcal{A}_\rho$ is the area of the wire cross section. In particular, for natural Si and Ge dots with $N\approx 10^4$ atoms [13,43,44], we find $\bar{\tau}_{\rm Si}\approx 0.36$ μs and $\bar{\tau}_{\rm Ge}\approx 0.11$ μs [63]. The dimensionless diagonal elements of Σ are

$$\sigma_x = \sigma_x^0, \quad \text{and} \quad \sigma_{y,z} = \sigma_M + e^{-(2l_z^2/l_{\rm SO}^2)}(\sigma_{y,z}^0 - \sigma_M), \tag{5}$$

and at $l_{\rm SO}^{-1} = 0$ they attain the values

$$\sigma_{x,y}^0 = \mathcal{A}_\rho\int d\boldsymbol{\rho}(|\psi_L|^4 + 3|\psi_L\psi_H|^2 \pm 2\sqrt{3}\mathrm{Re}[\psi_L^3\psi_H]), \tag{6a}$$

$$\sigma_z^0 = \mathcal{A}_\rho\int d\boldsymbol{\rho}\left(\frac{3}{2}|\psi_H|^2 - \frac{1}{2}|\psi_L|^2\right)^2. \tag{6b}$$

The DRSOI renormalizes $\sigma_{y,z}$ to the mean value $\sigma_M = (\sigma_y^0 + \sigma_z^0)/2$: this renormalization has important consequences on the qubit dynamics. The dependence of σ_i^0 on strain [64–68], on the direction of the field, and on extra valence bands is discussed in Sec. I B of [58].

Tunable hyperfine noise in spin qubits.—Because of the anisotropy of the hyperfine interactions, the spin dynamics strongly depends on the direction of the external fields. For simplicity, we consider $\mathbf{B}$ aligned along the confinement axes, such that $\boldsymbol{b}\|\mathbf{B}$ [69–72], and we analyze the dephasing of an idle qubit by finding the transition probability $P(t) = \langle|\langle -|e^{-iH_Q t/\hbar}|+\rangle|^2\rangle_g$ between the states $|\pm\rangle = (|0\rangle \pm |1\rangle)/\sqrt{2}$. Here, $|0,1\rangle$ are eigenstates of $\boldsymbol{b}\cdot\boldsymbol{\sigma}$ and the outer brackets indicate the average of $\boldsymbol{h}$ over a Gaussian distribution with covariance Σ [29,32,62,73].

For typical values $|\mathbf{B}|\sim 100$ mT, the hyperfine broadening is small, i.e., $|\boldsymbol{b}|\bar{\tau}/\hbar\sqrt{\sigma_i} \gg 1$, and

$$P(t) \approx \frac{1}{2} - \frac{1}{2}\frac{e^{-(t^2/2T_0^2)}\cos[\omega_B t + \phi(t)/2]}{\sqrt{4}(1+t^2/\tau_1^2)(1+t^2/\tau_2^2)}, \tag{7}$$

where $\phi(t) = \arctan(t/\tau_1) + \arctan(t/\tau_2)$. The hyperfine interactions parallel to $\boldsymbol{b}$ dampen the coherent spin precession with frequency $\omega_B = |\boldsymbol{b}|/\hbar$ by a Gaussian factor

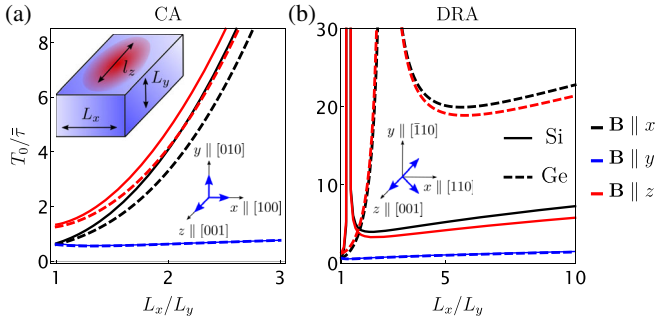

FIG. 1. Gaussian decay time T_0 in idle qubits in rectangular wires. We examine Si (solid lines) and Ge (dashed lines) dots when $E_y = 0$ and show T_0 for different directions of $\mathbf{B}$ as a function of L_x/L_y. In (a) and (b), we study wires grown along the CA and DRA, respectively. Confinement (crystallographic) axes are shown with black (blue) arrows.

with time scale $T_0 = \bar{\tau}/\sqrt{\sigma_\parallel}$, while the transverse interactions cause a power law decay with time scales $\tau_i = \omega_B \bar{\tau}^2/\sigma_\perp^i$ [27,29]. We call $\sigma_\parallel$ and $\sigma_\perp^{1,2}$ the dimensionless diagonal elements of Σ in Eq. (5) parallel and perpendicular to $\boldsymbol{b}$, respectively. Equation (7) is derived in Sec. II of [58], including also arbitrary field directions.

The power law tail is observable when $\tau_{1,2}/T_0 = \omega_B \bar{\tau} \sqrt{\sigma_\parallel}/\sigma_\perp^{1,2} \lesssim 1$, a condition that requires highly anisotropic hyperfine interactions when ω_B is in the GHz range. This anisotropy can be engineered by the confinement potential. For example, in rectangular wires [10] grown along the crystallographic axes (CAs), high aspect ratios $L_x/L_y \gg 1$ enable Ising hyperfine interactions $\propto h_y \sigma_y$ because the ground state comprises HHs polarized along the tighter confinement direction [26,27,29,30]. In Fig. 1(a), we show that the anisotropy decreases in typical Si and Ge wires where $L_x \sim L_y$, resulting in a fast Gaussian qubit decay for any direction of $\mathbf{B}$. In particular, at $L_x = L_y$ the Gaussian times T_0^i at $\mathbf{B} \| i = \{x, y, z\}$ are related by $T_0^x = T_0^y \approx T_0^z/2$, consistent with LH dots [30].

The hyperfine interactions are strikingly different when the cross section is rotated by $\pi/4$ with respect to z, as illustrated in Fig. 1(b). We call this orientation direct Rashba axes (DRAs) [45] because it guarantees the largest DRSOI in wires [8,9,72]. First, because of the sizeable HH-LH mixing even in planar heterostructures, yielding DRSOI [74], the hyperfine interactions are non-Ising at $L_x/L_y \gg 1$. The hyperfine anisotropy is still pronounced in wide Ge wires, but it decreases notably in Si, where the spin decay remains Gaussian with times T_0^i of hundreds of nanoseconds. Surprisingly, however, we find that the interplay of confinement potential and anisotropies of H_{LK} [8,53], restores Ising interactions at specific aspect ratios $L_x/L_y \approx 1.3(2.7)$ in Si (Ge). At these points the system has a HH-like ground state polarized along y and $T_0 \to \infty$ when $\mathbf{B} \perp y$, see Fig. 1(b), resulting in sweet spots

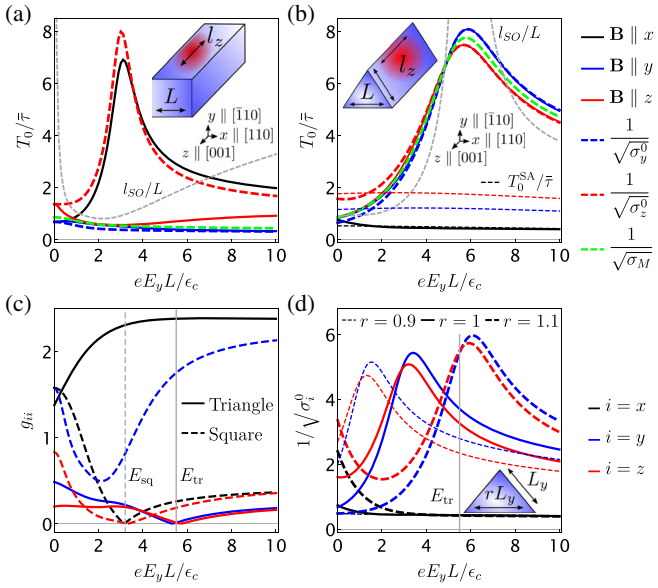

FIG. 2. Tunability of the hyperfine interactions. In (a) and (b), we show T_0 against E_y in Si wires grown along the DRA with square and equilateral triangular cross sections, respectively. E_y is measured in units of $\epsilon_c/eL \approx 3.22 \times (L/10\ \mathrm{nm})^{-3}\ \mathrm{V}/\mu\mathrm{m}$. Solid (dashed) lines represent results that include (neglect) DRSOI, see Eq. (5). In (b) we include the decay times T_0^{SA} of qubits in SA wires (thin dashed lines); l_{SO}/L is shown in dashed gray lines. In (c), we show the g factors in triangular and square wire qubits. Black, blue, red lines correspond to $\mathbf{B}$ aligned to x, y, z direction, respectively, and we use $l_z = L$. In (d), we include high energy states in triangular wires and compare cross sections having different aspect ratios r and the same area $\mathcal{A}_\rho = \sqrt{3}L^2/4$. Here, $L = 30$ nm.

where the qubit lifetime is largely enhanced and where the spin decay has a slow power-law tail with a longer timescale $\tau_1 = \omega_B \bar{\tau}^2/\sigma_y$ of tens of microseconds.

The presence of sweet spots for certain L_x/L_y suggests that the anisotropy of the hyperfine interactions could also be externally controlled by an electric field E_y, which compresses the wave function to the upper boundary of the wire. In Fig. 2(a), we study a square Si DRA wire with side L, and we show the effects of the E_y modulation of the wave function width on $T_0^{x,y,z}$ by solid black, dashed blue, and dashed red lines, respectively. A similar analysis for cylindrical Ge-Si core-shell nanowires is provided in Sec. I B of [58]. As anticipated, we observe the appearance of working points at $E_{\mathrm{sq}} \approx 3.1\epsilon_c/eL$ where hyperfine noise is suppressed by $\sim$20 times when $\mathbf{B} \perp y$, as seen by comparing the blue curves to the black and dashed red ones in Fig. 2(a). Here, $\epsilon_c = \hbar^2\pi^2\gamma_1/mL^2$, and for typical wires with $L = 20$ nm, the field $E_{\mathrm{sq}} \approx 1.25\ \mathrm{V}/\mu\mathrm{m}$ is experimentally accessible.

However, E_y also produces a large DRSOI [8,9], that does not affect T_0^x but strongly reduces T_0^z at E_{sq}, yielding $T_0^z \approx T_0^y \approx \bar{\tau}/\sqrt{\sigma_M} \ll T_0^x$, see Eq. (5) and the solid lines in

Fig. 2(a). As a consequence, in this system the hyperfine sweet spot remains only when $\mathbf{B}\|x$. We note that this field direction is useful to store information, but it is incompatible with EDSR, that requires that the Zeeman and spin-orbit fields are perpendicular to each other [16].

Strikingly, this issue is resolved in Si DRA FinFETs with triangular cross section [13,43–45], where the hyperfine sweet spots appear when $\mathbf{B}\perp x$. In fact, as shown in Fig. 2(b), the field directions minimizing the hyperfine noise depend on the shape of the cross section, and in contrast to square wires, in triangular fins $T_0^{y,z} \gtrsim 18 T_0^x$ at $E_{\rm tr} \approx 5.9\epsilon_c/eL$. Here, E_y pushes the wave function to a corner, favoring a HH polarization along x, see Sec. I B of [58]. More remarkably, because triangular wires lack inversion symmetry [45], the DRSOI $\propto l_{\rm SO}^{-1}$ is also switched off close to $E_{\rm tr}$ [dashed gray line in Fig. 2(b)], resulting in a highly coherent qubit, largely unaffected by both hyperfine *and* charge noise [45]. To drive these qubits, it suffices to switch on the DRSOI by tuning E_y with experimentally less demanding all-electric protocols.

In Fig. 2(b), we also compare the hyperfine noise in DRA FinFETs and in state-of-the-art devices [13,43,44], where the fins are grown along the standard axes (SAs) $z\|[110]$ and $y\|[100]$. In this case, we estimate $T_0^{\rm SA} \approx 0.2$–0.6 μs depending on the direction of $\mathbf{B}$, in reasonable agreement with experiments [13]. At the sweet spot DRA fins yield $\max(T_0^{\rm DRA}) \approx 5\max(T_0^{\rm SA})$. We emphasize that because $\bar{\tau} \propto 1/\sqrt{\nu}$ [see Eq. (4)], the hyperfine noise in DRA wires is comparable to the noise in isotopically purified SA wires, where $\nu_{\rm Si}^{\rm iso} = 800$ ppm [20,21] and the decay time $\max(T_0^{\rm SA})$ is 7.5 times longer than in natural Si.

We note that the position of the hyperfine sweet spots coincides with a minimal value of the g factor and with a small Zeeman energy, see Fig. 2(c). However, the hyperfine noise is suppressed in a broader range of E_y in the vicinity of $E_{\rm sq}$ and $E_{\rm tr}$, where the g factor is sizable. We find also that the hyperfine sweet spots persist when high energy valence bands are considered [58] and are robust against small variations of the aspect ratio r of the triangular cross section. In these cases, as shown in Fig. 2(d), the sweet spots are shifted to different values of E_y. Interestingly, when $r > 1$, we observe a cross-over between a regime where $T_0^x \ll T_0^y$ as in equilateral triangles to a regime where $T_0^x \gg T_0^y$ as in square wires. Similar transitions can be induced by strain, as discussed in Sec. I B of [58].

Hyperfine noise during qubit operations.—The DRSOI enables fast Rabi oscillations and qubit operations via EDSR [16]. Neglecting small hyperfine-induced EDSR terms [62,75], this effect originates from an ac electric field applied along the wire, that shifts the dot from its static position by $d(t) = d_0 \sin(\omega_D t)$. To obtain the fastest oscillations, we consider here a Zeeman field $\boldsymbol{b} = \hbar\omega_B[0, \sin(\theta_B), \cos(\theta_B)]$, perpendicular to the DRSOI, and we work at resonance $\omega_B = \omega_D$. In a frame moving with the dot, $\boldsymbol{h}$ becomes time-dependent $\boldsymbol{h}(t)$ because $\Gamma(\mathbf{r}_k) \to \Gamma[\mathbf{r}_k + d(t)\mathbf{e}_z]$, see Eq. (3), and the spin dynamic changes drastically [76,77]. Moving to a frame rotating with frequency ω_D around $\boldsymbol{b}$, and in the rotating wave approximation, only a few Fourier components $\boldsymbol{h}^m = \omega_D \int_0^{2\pi/\omega_D} dt e^{im\omega_D t}\boldsymbol{h}(t)/2\pi$ contribute [76], and

$$H_R \approx \frac{\hbar\omega_R + h_\perp^1}{2}\sigma_x + \frac{h_\parallel^0}{2}\sigma_z. \tag{8}$$

The Rabi frequency is $\omega_R = \omega_D d_0/l_{\rm SO}$, $h_\parallel^0 = h_y^0 \sin(\theta_B) + h_z^0\cos(\theta_B)$, and $h_\perp^1 = h_y^1\cos(\theta_B) - h_z^1\sin(\theta_B)$. The terms discarded are negligible for small but finite drive, with $d_0 \gtrsim l_{\rm SO}\sqrt{\sigma_i}/\omega_B\bar{\tau}$, see Sec. I C of [58]. A generalization of Eq. (8), valid off resonance, is also derived in [58].

In hole dots, $l_{\rm SO} \sim 10$ nm [13,14] is rather short and small driving amplitudes $d_0/l_z \ll 1$ suffice for fast qubit manipulation. In this case, the covariance of $\boldsymbol{h}$ is

$$\Sigma^R = \frac{\hbar^2}{\bar{\tau}^2}\begin{pmatrix} \frac{d_0^2}{4l_z^2}[\sigma_\perp + \frac{4l_z^2}{l_{\rm SO}^2}\sigma_M] & 0 & -\frac{d_0}{l_{\rm SO}}\sigma_M \\ 0 & 0 & 0 \\ -\frac{d_0}{l_{\rm SO}}\sigma_M & 0 & \sigma_\parallel \end{pmatrix}, \tag{9}$$

where $\sigma_{\perp,\parallel} = \sigma_{y,z} \mp (\sigma_y - \sigma_z)\sin(\theta_B)^2$ are the components of the hyperfine noise parallel and perpendicular to $\boldsymbol{b}$, respectively [see Eq. (5)].

From Eqs. (8) and (9), one expects a Gaussian and a power-law decay determined by Σ_{11}^R and Σ_{33}^R, respectively. We emphasize that because of the weak driving the Gaussian timescale is enlarged by l_z/d_0, thus enhancing the coherence of qubit operations [76] to a level comparable to magnetically driven spins [78]. Also, the power-law timescale $\tau_1 = \omega_R\bar{\tau}^2/\sigma_\parallel \propto d_0$ is now comparable to the Gaussian timescale even for rather isotropic hyperfine interactions, in striking contrast to idle qubits.

More precisely, the spin-flip probability averaged over a Gaussian distributed field $\boldsymbol{h}$ with covariance Σ^R is [58]

$$P_R(t) \approx \frac{1}{2} - \frac{1}{2}\frac{e^{-[(t^2)/2T_R^2(t)]}\cos[\omega_R t + \phi_R(t)/2]}{\sqrt[4]{1 + t^2/\tau_1^2}}, \tag{10}$$

with $\phi_R(t) = \arctan(t/\tau_1) - \omega_R t^3(\Sigma_{13}^R/\Sigma_{33}^R)^2/(t^2 + \tau_1^2)$. Surprisingly, we observe that the strong DRSOI not only quantitatively renormalizes Σ_{ii}^R, but also introduces off-diagonal elements $\Sigma_{13}^R = \Sigma_{31}^R$ that alter the spin dynamics qualitatively. In particular, they result in a time-dependent Gaussian timescale

$$\frac{1}{T_R^2(t)} = \frac{1}{T_<^2} - \frac{1}{\bar{\tau}^2}\frac{d_0^2}{l_{\rm SO}^2}\frac{\sigma_M^2}{\sigma_\parallel}\frac{t^2}{t^2 + \tau_1^2}, \tag{11}$$

that interpolates between the short time $T_< = \hbar/\sqrt{\Sigma_{11}^R}$, when $t \ll \tau_1$, to the longer time $T_> = (T_<^{-2} - \sigma_M^2 d_0^2/\bar{\tau}^2 l_{\rm SO}^2\sigma_\parallel)^{-1/2} > T_<$, when $t \gg \tau_1$.

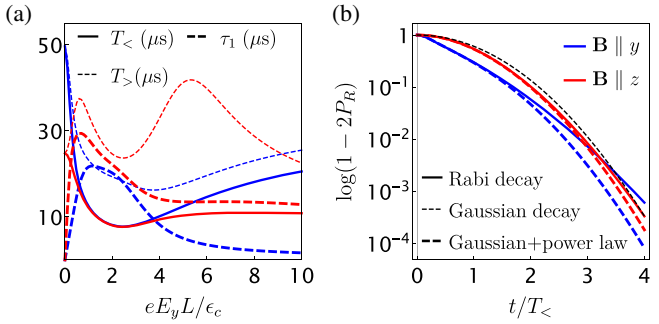

FIG. 3. Spin decay during qubit operations. In (a) we show the relevant decay times when $\mathbf{B}\|y$ (blue) and $\mathbf{B}\|z$ (red) of a qubit in a Si square wire grown along the DRA. Here, $l_z = L$, $\omega_B/2\pi = 3$ GHz, $N = 10^4$, and $d_0 = 0.02l_z$, resulting in $\omega_R^{\max}/2\pi \approx 75$ MHz. In (b) we consider $E_y = 6\epsilon_c/eL$ and study the spin decay of the Rabi oscillations and its deviation from purely Gaussian and power-law scaling.

A comparison between different timescales in a typical Rabi experiment is shown in Fig. 3(a) and we note that in this case, the decay times are of tens of microseconds, much longer than in idle qubits. Rabi oscillations with similarly high coherence were recently observed in hole Si FinFETs [13]. We also predict that at the large values of DRSOI achieved in current experiments [12–15] the interplay between the different decay times will yield measurable effects, see Fig. 3(b), further decreasing the effect of hyperfine noise during qubit operations.

In conclusion, we studied the hyperfine interactions of a hole spin qubit in elongated quantum dots and we showed that they can be tuned over a wide range of parameters by device design and by external electric fields. In certain devices, this tunability enables sweet spots where the hyperfine noise is strongly reduced and becomes comparable to isotopically purified materials. Remarkably, in Si FinFETs charge and hyperfine noises are both suppressed at these sweet spots, pushing this architecture towards new coherence standards. Combined with the high speed and fidelity of operations, these highly coherent qubits can be reliable building blocks for scalable quantum computers.

We thank Bence Hetényi and Dmitry Miserev for useful discussions. This work was supported by the Swiss National Science Foundation and NCCR SPIN.

*stefano.bosco@unibas.ch

[1] G. Scappucci, C. Kloeffel, F. A. Zwanenburg, D. Loss, M. Myronov, J.-J. Zhang, S. De Franceschi, G. Katsaros, and M. Veldhorst, The germanium quantum information route, Nat. Rev. Mater. **6**, 926 (2021).

[2] C. Kloeffel and D. Loss, Prospects for spin-based quantum computing in quantum dots, Annu. Rev. Condens. Matter Phys. **4**, 51 (2013).

[3] N. W. Hendrickx, W. I. L. Lawrie, M. Russ, F. van Riggelen, S. L. de Snoo, R. N. Schouten, A. Sammak, G. Scappucci, and M. Veldhorst, A four-qubit germanium quantum processor, Nature (London) **591**, 580 (2021).

[4] D. Jirovec, A. Hofmann, A. Ballabio, P. M. Mutter, G. Tavani, M. Botifoll, A. Crippa, J. Kukucka, O. Sagi, F. Martins, J. Saez-Mollejo, I. Prieto, M. Borovkov, J. Arbiol, D. Chrastina, G. Isella, and G. Katsaros, A singlet-triplet hole spin qubit in planar Ge, Nat. Mater. **20**, 1106 (2021).

[5] N. W. Hendrickx, W. I. L. Lawrie, L. Petit, A. Sammak, G. Scappucci, and M. Veldhorst, A single-hole spin qubit, Nat. Commun. **11**, 3478 (2020).

[6] C. Kloeffel, M. Trif, and D. Loss, Strong spin-orbit interaction and helical hole states in Ge/Si nanowires, Phys. Rev. B **84**, 195314 (2011).

[7] C. Kloeffel, M. Trif, P. Stano, and D. Loss, Circuit QED with hole-spin qubits in Ge/Si nanowire quantum dots, Phys. Rev. B **88**, 241405(R) (2013).

[8] C. Kloeffel, M. J. Rančić, and D. Loss, Direct Rashba spin-orbit interaction in Si and Ge nanowires with different growth directions, Phys. Rev. B **97**, 235422 (2018).

[9] S. Bosco, M. Benito, C. Adelsberger, and D. Loss, Squeezed hole spin qubits in Ge quantum dots with ultrafast gates at low power, Phys. Rev. B **104**, 115425 (2021).

[10] R. Maurand, X. Jehl, D. Kotekar-Patil, A. Corna, H. Bohuslavskyi, R. Laviéville, L. Hutin, S. Barraud, M. Vinet, M. Sanquer, and S. De Franceschi, A CMOS silicon spin qubit, Nat. Commun. **7**, 13575 (2016).

[11] N. Hendrickx, D. Franke, A. Sammak, G. Scappucci, and M. Veldhorst, Fast two-qubit logic with holes in germanium, Nature (London) **577**, 487 (2020).

[12] H. Watzinger, J. Kukučka, L. Vukušić, F. Gao, T. Wang, F. Schäffler, J.-J. Zhang, and G. Katsaros, A germanium hole spin qubit, Nat. Commun. **9**, 3902 (2018).

[13] L. C. Camenzind, S. Geyer, A. Fuhrer, R. J. Warburton, D. M. Zumbühl, and A. V. Kuhlmann, A spin qubit in a fin field-effect transistor, arXiv:2103.07369.

[14] F. N. M. Froning, L. C. Camenzind, O. A. H. van der Molen, A. Li, E. P. A. M. Bakkers, D. M. Zumbühl, and F. R. Braakman, Ultrafast hole spin qubit with gate-tunable spin–orbit switch functionality, Nat. Nanotechnol. **16**, 308 (2021).

[15] K. Wang, G. Xu, F. Gao, H. Liu, R.-L. Ma, X. Zhang, T. Zhang, G. Cao, T. Wang, J.-J. Zhang, X. Hu, H.-W. Jiang, H.-O. Li, G.-C. Guo, and G.-P. Guo, Ultrafast operations of a hole spin qubit in Ge quantum dot, arXiv:2006.12340.

[16] V. N. Golovach, M. Borhani, and D. Loss, Electric-dipole-induced spin resonance in quantum dots, Phys. Rev. B **74**, 165319 (2006).

[17] D. V. Bulaev and D. Loss, Electric Dipole Spin Resonance for Heavy Holes in Quantum Dots, Phys. Rev. Lett. **98**, 097202 (2007).

[18] A. Crippa, R. Maurand, L. Bourdet, D. Kotekar-Patil, A. Amisse, X. Jehl, M. Sanquer, R. Laviéville, H. Bohuslavskyi, L. Hutin, S. Barraud, M. Vinet, Y.-M. Niquet, and S. De Franceschi, Electrical Spin Driving by g-Matrix Modulation in Spin-Orbit Qubits, Phys. Rev. Lett. **120**, 137702 (2018).

[19] V. P. Michal, B. Venitucci, and Y.-M. Niquet, Longitudinal and transverse electric field manipulation of hole spin-orbit

qubits in one-dimensional channels, Phys. Rev. B **103**, 045305 (2021).
[20] M. Veldhorst, J. Hwang, C. Yang, A. Leenstra, B. de Ronde, J. Dehollain, J. Muhonen, F. Hudson, K. M. Itoh, A. Morello, and A. S. Dzurak, An addressable quantum dot qubit with fault-tolerant control-fidelity, Nat. Nanotechnol. **9**, 981 (2014).
[21] J. Yoneda, K. Takeda, T. Otsuka, T. Nakajima, M. R. Delbecq, G. Allison, T. Honda, T. Kodera, S. Oda, Y. Hoshi, N. Usami, K. M. Itoh, and S. Tarucha, A quantum-dot spin qubit with coherence limited by charge noise and fidelity higher than 99.9%, Nat. Nanotechnol. **13**, 102 (2018).
[22] A. M. Tyryshkin, S. Tojo, J. J. Morton, H. Riemann, N. V. Abrosimov, P. Becker, H.-J. Pohl, T. Schenkel, M. L. Thewalt, K. M. Itoh, and S. A. Lyon, Electron spin coherence exceeding seconds in high-purity silicon, Nat. Mater. **11**, 143 (2012).
[23] R. J. Warburton, Single spins in self-assembled quantum dots, Nat. Mater. **12**, 483 (2013).
[24] D. Brunner, B. D. Gerardot, P. A. Dalgarno, G. Wst, K. Karrai, N. G. Stoltz, P. M. Petroff, and R. J. Warburton, A coherent single-hole spin in a semiconductor, Science **325**, 70 (2009).
[25] B. D. Gerardot, D. Brunner, P. A. Dalgarno, P. Öhberg, S. Seidl, M. Kroner, K. Karrai, N. G. Stoltz, P. M. Petroff, and R. J. Warburton, Optical pumping of a single hole spin in a quantum dot, Nature (London) **451**, 441 (2008).
[26] P. Machnikowski, K. Gawarecki, and L. Cywiński, Hyperfine interaction for holes in quantum dots: $k \cdot p$ model, Phys. Rev. B **100**, 085305 (2019).
[27] C. Testelin, F. Bernardot, B. Eble, and M. Chamarro, Hole–spin dephasing time associated with hyperfine interaction in quantum dots, Phys. Rev. B **79**, 195440 (2009).
[28] B. Eble, C. Testelin, P. Desfonds, F. Bernardot, A. Balocchi, T. Amand, A. Miard, A. Lemaître, X. Marie, and M. Chamarro, Hole–Nuclear Spin Interaction in Quantum Dots, Phys. Rev. Lett. **102**, 146601 (2009).
[29] J. Fischer, W. A. Coish, D. V. Bulaev, and D. Loss, Spin decoherence of a heavy hole coupled to nuclear spins in a quantum dot, Phys. Rev. B **78**, 155329 (2008).
[30] P. Philippopoulos, S. Chesi, and W. A. Coish, First-principles hyperfine tensors for electrons and holes in gaas and silicon, Phys. Rev. B **101**, 115302 (2020).
[31] P. Philippopoulos, Hyperfine and spin-orbit interactions in semiconductor nanostructures, Ph.D. thesis, McGill University, 2020.
[32] I. A. Merkulov, A. L. Efros, and M. Rosen, Electron spin relaxation by nuclei in semiconductor quantum dots, Phys. Rev. B **65**, 205309 (2002).
[33] A. V. Khaetskii, D. Loss, and L. Glazman, Electron Spin Decoherence in Quantum Dots due to Interaction with Nuclei, Phys. Rev. Lett. **88**, 186802 (2002).
[34] W. A. Coish and D. Loss, Hyperfine interaction in a quantum dot: Non-Markovian electron spin dynamics, Phys. Rev. B **70**, 195340 (2004).
[35] T. Belhadj, T. Amand, A. Kunold, C.-M. Simon, T. Kuroda, M. Abbarchi, T. Mano, K. Sakoda, S. Kunz, X. Marie, and B. Urbaszek, Impact of heavy hole-light hole coupling on optical selection rules in GaAs quantum dots, Appl. Phys. Lett. **97**, 051111 (2010).
[36] F. H. L. Koppens, D. Klauser, W. A. Coish, K. C. Nowack, L. P. Kouwenhoven, D. Loss, and L. M. K. Vandersypen, Universal Phase Shift and Nonexponential Decay of Driven Single-Spin Oscillations, Phys. Rev. Lett. **99**, 106803 (2007).
[37] W. A. Coish and D. Loss, Singlet-triplet decoherence due to nuclear spins in a double quantum dot, Phys. Rev. B **72**, 125337 (2005).
[38] J. Fischer and D. Loss, Hybridization and Spin Decoherence in Heavy-Hole Quantum Dots, Phys. Rev. Lett. **105**, 266603 (2010).
[39] F. Maier and D. Loss, Effect of strain on hyperfine-induced hole-spin decoherence in quantum dots, Phys. Rev. B **85**, 195323 (2012).
[40] D. Klauser, W. A. Coish, and D. Loss, Nuclear spin state narrowing via gate-controlled Rabi oscillations in a double quantum dot, Phys. Rev. B **73**, 205302 (2006).
[41] J. H. Prechtel, A. V. Kuhlmann, J. Houel, A. Ludwig, S. R. Valentin, A. D. Wieck, and R. J. Warburton, Decoupling a hole spin qubit from the nuclear spins, Nat. Mater. **15**, 981 (2016).
[42] E. A. Chekhovich, M. N. Makhonin, A. I. Tartakovskii, A. Yacoby, H. Bluhm, K. C. Nowack, and L. M. K. Vandersypen, Nuclear spin effects in semiconductor quantum dots, Nat. Mater. **12**, 494 (2013).
[43] S. Geyer, L. C. Camenzind, L. Czornomaz, V. Deshpande, A. Fuhrer, R. J. Warburton, D. M. Zumbühl, and A. V. Kuhlmann, Self-aligned gates for scalable silicon quantum computing, Appl. Phys. Lett. **118**, 104004 (2021).
[44] A. V. Kuhlmann, V. Deshpande, L. C. Camenzind, D. M. Zumbühl, and A. Fuhrer, Ambipolar quantum dots in undoped silicon fin field-effect transistors, Appl. Phys. Lett. **113**, 122107 (2018).
[45] S. Bosco, B. Hetényi, and D. Loss, Hole spin qubits in Si FinFETs with fully tunable spin-orbit coupling and sweet spots for charge noise, PRX Quantum **2**, 010348 (2021).
[46] M. J. Rančić and G. Burkard, Interplay of spin-orbit and hyperfine interactions in dynamical nuclear polarization in semiconductor quantum dots, Phys. Rev. B **90**, 245305 (2014).
[47] B. Hensen, W. W. Huang, C.-H. Yang, K. W. Chan, J. Yoneda, T. Tanttu, F. E. Hudson, A. Laucht, K. M. Itoh, T. D. Ladd, A. Morello, and A. S. Dzurak, A silicon quantum-dot-coupled nuclear spin qubit, Nat. Nanotechnol. **15**, 13 (2020).
[48] B. E. Kane, A silicon-based nuclear spin quantum computer, Nature (London) **393**, 133 (1998).
[49] T. D. Ladd, J. R. Goldman, F. Yamaguchi, Y. Yamamoto, E. Abe, and K. M. Itoh, All-Silicon Quantum Computer, Phys. Rev. Lett. **89**, 017901 (2002).
[50] J. J. Pla, F. A. Mohiyaddin, K. Y. Tan, J. P. Dehollain, R. Rahman, G. Klimeck, D. N. Jamieson, A. S. Dzurak, and A. Morello, Coherent Control of a Single ^{29}Si Nuclear Spin Qubit, Phys. Rev. Lett. **113**, 246801 (2014).
[51] L. M. K. Vandersypen, H. Bluhm, J. S. Clarke, A. S. Dzurak, R. Ishihara, A. Morello, D. J. Reilly, L. R. Schreiber, and M. Veldhorst, Interfacing spin qubits in quantum dots and donors—hot, dense, and coherent, npj Quantum Inf. **3**, 34 (2017).

[52] J. J. Pla, K. Y. Tan, J. P. Dehollain, W. H. Lim, J. J. L. Morton, D. N. Jamieson, A. S. Dzurak, and A. Morello, A single-atom electron spin qubit in silicon, Nature (London) **489**, 541 (2012).

[53] R. Winkler, *Spin–Orbit Coupling Effects in Two-Dimensional Electron and Hole Systems*, edited by G. Höhler, J. H. Kühn, T. Müller, J. Trümper, A. Ruckenstein, P. Wölfle, and F. Steiner, Springer Tracts in Modern Physics Vol. 191 (Springer Berlin Heidelberg, Berlin, Heidelberg, 2003).

[54] H. Watzinger, C. Kloeffel, L. Vukusic, M. D. Rossell, V. Sessi, J. Kukucka, R. Kirchschlager, E. Lausecker, A. Truhlar, M. Glaser, A. Rastelli, A. Fuhrer, D. Loss, and G. Katsaros, Heavy-hole states in germanium hut wires, Nano Lett. **16**, 6879 (2016).

[55] P. Fallahi, S. T. Yılmaz, and A. Imamoğlu, Measurement of a Heavy-Hole Hyperfine Interaction in InGaAs Quantum Dots Using Resonance Fluorescence, Phys. Rev. Lett. **105**, 257402 (2010).

[56] E. A. Chekhovich, A. B. Krysa, M. S. Skolnick, and A. I. Tartakovskii, Direct Measurement of the Hole-Nuclear Spin Interaction in Single InP/GaInP Quantum Dots Using Photoluminescence Spectroscopy, Phys. Rev. Lett. **106**, 027402 (2011).

[57] P. Philippopoulos, S. Chesi, J. Salfi, S. Rogge, and W. A. Coish, Hole spin echo envelope modulations, Phys. Rev. B **100**, 125402 (2019).

[58] See Supplemental Material at http://link.aps.org/supplemental/10.1103/PhysRevLett.127.190501 for an explicit derivation of the general spin-flip probability and of the covariance matrix of the hyperfine interactions in idle and driven hole spin qubits. We also include a discussion on other experimentally relevant platforms, and on the effect of strain and of arbitrary field directions.

[59] C. Adelsberger, M. Benito, S. Bosco, J. Klinovaja, and D. Loss, Hole spin qubits in Ge nanowire quantum dots: Interplay of orbital magnetic field, strain, and growth direction (to be published).

[60] F. N. M. Froning, M. J. Rančić, B. Hetényi, S. Bosco, M. K. Rehmann, A. Li, E. P. A. M. Bakkers, F. A. Zwanenburg, D. Loss, D. M. Zumbühl, and F. R. Braakman, Strong spin-orbit interaction and g-factor renormalization of hole spins in Ge/Si nanowire quantum dots, Phys. Rev. Research **3**, 013081 (2021).

[61] M. Trif, V. N. Golovach, and D. Loss, Spin dynamics in InAs nanowire quantum dots coupled to a transmission line, Phys. Rev. B **77**, 045434 (2008).

[62] E. I. Rashba, Theory of electric dipole spin resonance in quantum dots: Mean field theory with gaussian fluctuations and beyond, Phys. Rev. B **78**, 195302 (2008).

[63] We use $\nu_{\mathrm{Si}} = 4.7\%$, $I_{\mathrm{Si}} = 1/2$, $|A_k^{\mathrm{Si}}| = 1.67\ \mu$eV, and $\nu_{\mathrm{Ge}} = 7.7\%$, $I_{\mathrm{Ge}} = 9/2$, $|A_k^{\mathrm{Ge}}| = 0.73\ \mu$eV; A_k^i is related by $A_k^i \equiv 2A_{\parallel}^i/3$ to the quantity $A_{\parallel}^i$ estimated in [30,31] for Si and Ge, respectively.

[64] G. L. Bir and G. E. Pikus, *Symmetry and Strain-Induced Effects in Semiconductors* (Wiley, New York, 1974), Vol. 484.

[65] C. Kloeffel, M. Trif, and D. Loss, Acoustic phonons and strain in core/shell nanowires, Phys. Rev. B **90**, 115419 (2014).

[66] S. Liles, F. Martins, D. Miserev, A. Kiselev, I. Thorvaldson, M. Rendell, I. Jin, F. Hudson, M. Veldhorst, K. Itoh, O. P. Sushkov, T. D. Ladd, A. S. Dzurak, and A. R. Hamilton, Electrical control of the g-tensor of a single hole in a silicon MOS quantum dot, arXiv:2012.04985.

[67] T. Thorbeck and N. M. Zimmerman, Formation of strain-induced quantum dots in gated semiconductor nanostructures, AIP Adv. **5**, 087107 (2015).

[68] Y.-M. Niquet, C. Delerue, and C. Krzeminski, Effects of strain on the carrier mobility in silicon nanowires, Nano Lett. **12**, 3545 (2012).

[69] B. Hetényi, C. Kloeffel, and D. Loss, Exchange interaction of hole-spin qubits in double quantum dots in highly anisotropic semiconductors, Phys. Rev. Research **2**, 033036 (2020).

[70] L. Bellentani, M. Bina, S. Bonen, A. Secchi, A. Bertoni, S. Voinigescu, A. Padovani, L. Larcher, and F. Troiani, Towards hole-spin qubits in Si pMOSFETs within a planar CMOS foundry technology, arXiv:2106.04940.

[71] B. Venitucci, L. Bourdet, D. Pouzada, and Y.-M. Niquet, Electrical manipulation of semiconductor spin qubits within the g-matrix formalism, Phys. Rev. B **98**, 155319 (2018).

[72] B. Venitucci and Y.-M. Niquet, Simple model for electrical hole spin manipulation in semiconductor quantum dots: Impact of dot material and orientation, Phys. Rev. B **99**, 115317 (2019).

[73] J. M. Martinis, S. Nam, J. Aumentado, K. M. Lang, and C. Urbina, Decoherence of a superconducting qubit due to bias noise, Phys. Rev. B **67**, 094510 (2003).

[74] J.-X. Xiong, S. Guan, J.-W. Luo, and S.-S. Li, Emergence of strong tunable linear Rashba spin-orbit coupling in two-dimensional hole gases in semiconductor quantum wells, Phys. Rev. B **103**, 085309 (2021).

[75] E. A. Laird, C. Barthel, E. I. Rashba, C. M. Marcus, M. P. Hanson, and A. C. Gossard, Hyperfine-Mediated Gate-Driven Electron Spin Resonance, Phys. Rev. Lett. **99**, 246601 (2007).

[76] S. Chesi, L.-P. Yang, and D. Loss, Dephasing due to Nuclear Spins in Large-Amplitude Electric Dipole Spin Resonance, Phys. Rev. Lett. **116**, 066806 (2016).

[77] G. Széchenyi and A. Pályi, Maximal Rabi frequency of an electrically driven spin in a disordered magnetic field, Phys. Rev. B **89**, 115409 (2014).

[78] F. H. L. Koppens, C. Buizert, K. J. Tielrooij, I. T. Vink, K. C. Nowack, T. Meunier, L. P. Kouwenhoven, and L. M. K. Vandersypen, Driven coherent oscillations of a single electron spin in a quantum dot, Nature (London) **442**, 766 (2006).